THE JOURNAL OF PHYSICAL CHEMISTRY C

Article

Cite This: J. Phys. Chem. C 2019, 123, 13856−13862

pubs.acs.org/JPCC

Broadband and Polarization-Insensitive Absorption Based on a Set of Multisized Fabry−Perot-like Resonators

Sha Hu,[†,‡] Shengyan Yang,[†,‡] Zhe Liu,[†,§] Baogang Quan,[†] Junjie Li,[*,†,‡,∥] and Changzhi Gu[*,†,‡]

[†]Beijing National Laboratory for Condensed Matter Physics, Institute of Physics, Chinese Academy of Sciences, Beijing 100190, China

[‡]School of Physical Sciences, CAS Key Laboratory of Vacuum Physics, University of Chinese Academy of Sciences, Beijing 100049, China

[§]Niels Bohr Institute, University of Copenhagen, Blegdamsvej 17, Copenhagen DK-2100, Denmark

[∥]Songshan Lake Materials Laboratory, Dongguan 523808, Guangdong, China

ABSTRACT: We experimentally and theoretically demonstrate a broadband and polarization-insensitive truncated-cone-type multilayer metamaterial absorber in the near-IR to mid-IR range. Its fabrication process combines lithography and ion beam etching techniques, which have the advantages of both high throughput and nanoscale feature size. The absorption band could be experimentally tuned from near-IR to the mid-IR range by tailoring the geometric parameters, that is, bevel angle and bottom diameter. In theory, this multilayer structure can support the gap surface plasmon−polariton (G-SPP) mode to confine the electric field in all dielectric layers. Because of counter-propagating G-SPPs forming standing waves, the stronger electric field is confined in the dielectric layers like Fabry−Perot resonators. These multisized Fabry−Perot-like resonators can trap multiwavelength incident light, giving rise to high and broadband absorption. With the separation between two adjacent nanostructures decreasing , the leakage fields of G-SPP modes can couple with each other in the air gap, leading to a stronger field and higher absorption. This broadband metamaterial absorber could lead to various advanced applications, and its fabrication method provides a straightforward and mass-production strategy to fabricate multilayer metamaterials.

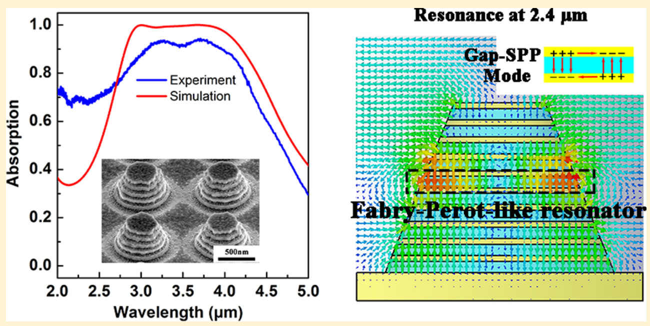

■ INTRODUCTION

Metamaterials, which are artificially engineered materials composed of subwavelength meta-atoms,[1] exhibit unusual and exotic electromagnetic properties, such as negative refraction,[3] superlens,[4] plasmon-induced transparency,[5] and strong polarization conversion[6] that are unavailable in naturally occurring materials.[2] However, these properties of specially designed metamaterials are limited by Ohmic losses, especially for metallic metamaterials at the infrared and optical frequencies. In contrast, metamaterials acting as perfect absorbers could take full advantage of the Ohmic losses, and the absorption performances could be significantly improved by tailoring unit cells and optimizing geometrical parameters.

Since the first demonstration of metamaterial-based absorbers by Landy et al.,[7] metamaterial absorbers have attracted tremendous research interest due to their great potential applications, such as solar energy harvesting,[8,9] thermal detectors,[10] and plasmonic sensors.[11−14] The unit cell of a metamaterial absorber was usually a sandwich structure that consisted of metallic patterns and metallic cut wires (or metallic boards) separated by a dielectric layer. This typical nanostructure array could achieve perfect absorption at a certain frequency,[7,15−17] which limited its practical applications. Subsequently, metamaterial absorbers with multi-band absorption have been developed by using building blocks with different geometries.[18−22] When the differences in geometrical parameters diminish, absorption resonances at very close-by frequencies could overlap to realize the broadband light trapping. Following this intuitive strategy, multiple metallic resonators with different sizes were placed in the same layer to increase the absorption bandwidth.[23−27] However, the operation bandwidth of these metamaterial absorbers is still limited by the density of absorption elements. Therefore, an alternative method of vertically stacking metal−dielectric pairs with slight size variation has been proposed to effectively broaden the absorption bandwidth.[28−34] Broadband microwave multilayered metamaterial absorbers have been fabricated by the milling process, whereas this method has difficulty in miniaturizing the structure to nanoscale and extending the absorption band to infrared regions.[28,29] Recently, focused ion beam (FIB)[33] and self-mask deposition[34] methods were introduced to fabricate polarization-dependent

Received: February 20, 2019
Revised: April 7, 2019
Published: April 29, 2019

DOI: 10.1021/acs.jpcc.9b01634
J. Phys. Chem. C 2019, 123, 13856−13862

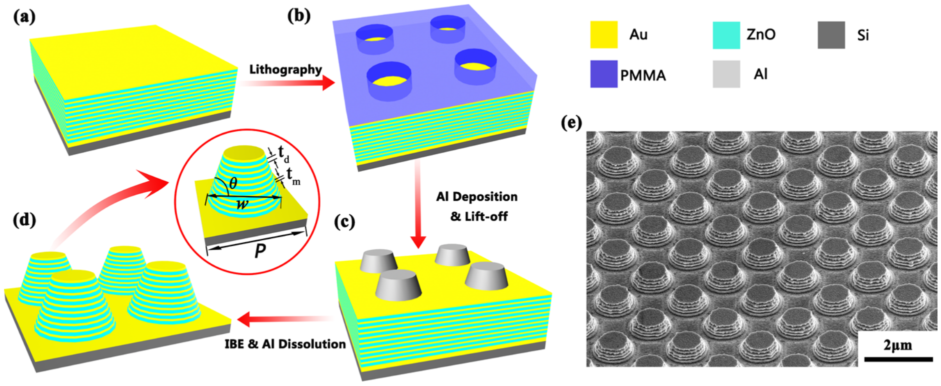

Figure 1. Schematic of the fabrication process and SEM image of the truncated-cone-type metamaterial. (a) Stacked Au−ZnO multifilms by magnetron sputtering. (b) Hole array in PMMA by lithography. (c) Aluminum tapered plate array on Au−ZnO multifilms by electron beam evaporation and lift-off processes. (d) Ion beam etching to obtain truncated-cone-type multilayer nanostructures. (e) 52°-tilted SEM image of the truncated-cone-type metamaterial with P = 1.5 μm and 5-pair Au−ZnO.

tapered hyperbolic metamaterial (HMM) absorbers. However, FIB technology has low fabrication efficiency and relatively low etching resolution due to charging effect on dielectric materials, whereas the self-mask deposition is limited by precise control of shadow evaporation and is also difficult to create various structural morphologies except for one-dimensional periodic structures. Therefore, it is important to develop an easily controllable and mass-production strategy to experimentally implement HMM absorbers at nanoscale. The broadband absorption of the multilayer tapered metamaterial absorber has already been interpreted with electric and magnetic resonant modes,[28,29,32] slow light effect,[31] and HMM waveguide modes.[33,34] However, the essential resonance mode and corresponding interaction mechanisms in the multilayer nanostructure resonators has remained elusive. Further, the metal−insulator−metal (MIM) structures have been studied based on the gap surface plasmon−polariton (G-SPP),[35−37] which can be reflected at the structure terminations. Because of constructive interferences of counter-propagating G-SPP modes, the MIM structure can be considered as a Fabry−Perot-like resonator.[38−40] This inspires us to apply Fabry−Perot-like resonance coupled by G-SPP modes on the broadband multilayered metamaterial absorber.

In this work, we demonstrate a flexible and mass-production fabrication method to realize a broadband, polarization-insensitive, and wide-angle truncated-cone-type metamaterial absorber (TCMA). The TCMAs are fabricated by ion beam etching (IBE) on a Au−ZnO multifilm, which has high fabrication efficiency and flexibility. Based on this fabrication technology, we design and fabricate a truncated-cone-type multilayered nanostructure array, and its absorption bandwidth could be effectively scaled and modulated from near-IR to mid-IR range by modifying the process parameters. To explore the essential resonance in the TCMA structure, it can be decomposed into a series of assumptive MIM resonators with varied diameters. These MIM resonators can support the G-SPP mode with a large mode-index and strong confinement in the dielectric layers. For tapered TCMA nanostructures, the G-SPP modes excited by broad incident waves can be stood due to the constructive interference between counter-propagating G-SPPs in the multisized Fabry−Perot-like resonators, giving rise to efficient trapping of broadband incident light. In order to understand the period effect, the field distributions of G-SPP modes in the interface between TCMA nanostructure and air gap are studied. With the separation between two adjacent nanostructures decreasing, the leakage field of G-SPP modes in the interfaces can couple with each other, leading to more electric field stored in the air gap and realize higher absorption.

■ EXPERIMENTAL METHODS

The truncated-cone-type multilayer metamaterials are fabricated by etching on Au−ZnO-stacked multilayered films to experimentally achieve broadband and polarization-insensitive absorption. The schematic of the fabrication process is shown in Figure 1. First, a gold film with a thickness of 100 nm was deposited on silicon substrate by magnetron sputtering to block light transmission. The ZnO and gold films were then alternately sputtered until the desired layer number was attained (Figure 1a). After spin-coating with resist, the multilayered Au−ZnO film was exposed by electron beam lithography, nanoimprint, laser direct writing, or ultraviolet (UV) exposure to form the hole arrays, as shown in Figure 1b. In the next step (Figure 1c), the hole pattern was transferred to aluminum truncated-cone-type array by the electron beam evaporation and lift-off processes. Subsequently, the IBE was performed to transfer the truncated-cone-type nanostructure to the Au−ZnO multilayered film (Figure 1d), whose bevel angles are mainly dependent on the bevel angle and thickness of deposited mask as well as the etching parameters of IBE (e.g., etching incidence angle and ion energy). It is worth noting that the tapered etching disk plays a pivotal role in forming the truncated-cone-type Au−ZnO multilayered nanostructures. Finally, the TCMA was obtained after removing the residual aluminum by tetramethylammonium hydroxide, which presents weak alkalinity and does not react chemically with Au and ZnO. The method of etching on multifilms can be effectively and flexibly applied to fabricate the multilayer metamaterials besides truncated-cone-type nanostructures. Comparing with other preparation methods of multilayer metamaterial absorbers,[33,34] the combination of lithography and IBE fabrication processes could achieve high throughput and create various structural morphologies simultaneously. The scanning electron microscopy (SEM) image of fabricated TCMA is shown in Figure 1e. The gold layer has a thickness of t_m, and the thickness for ZnO layer is t_d.

DOI: 10.1021/acs.jpcc.9b01634
J. Phys. Chem. C 2019, 123, 13856−13862

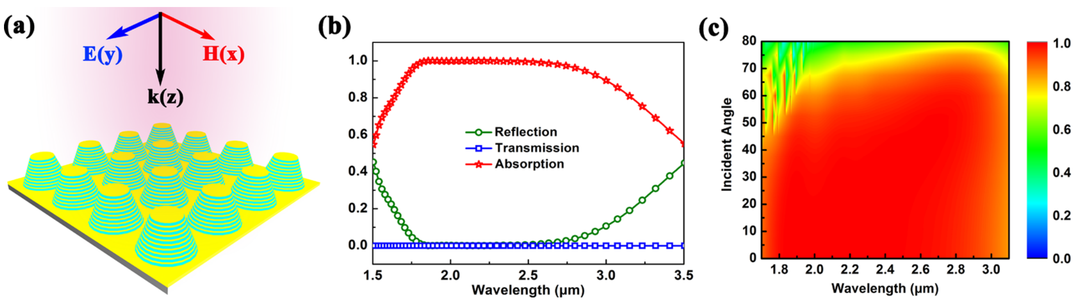

Figure 2. Simulated absorption spectra. (a) Diagram of the TCMA structure. (b) Calculated absorption spectrum for the TCMA absorber with number of metal−dielectric pairs, $N = 10$. Geometric parameters: $t_m = 20$ nm, $t_d = 40$ nm, $P = 1$ μm, $w = 800$ nm, $\theta = 68.2°$. (c) Absorption spectra for different incident angles.

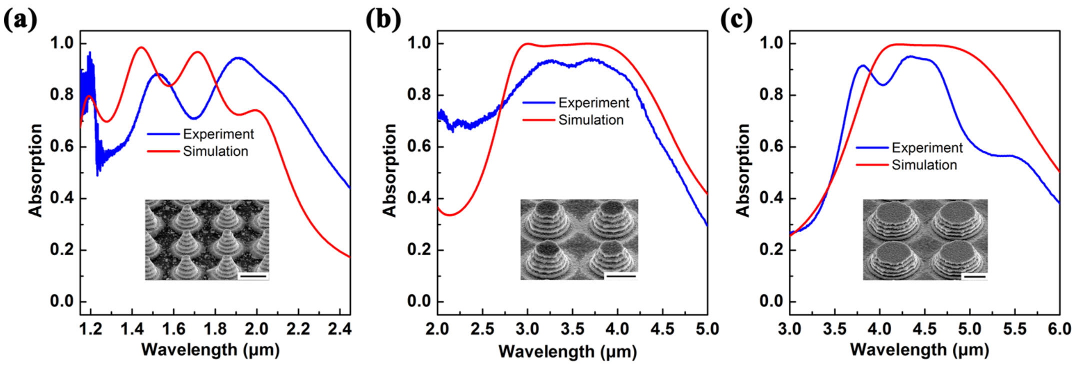

Figure 3. Measured (blue) and simulated (red) absorption spectra for multilayered TCMA absorbers with 5-pair Au−ZnO. The parameters of period, bottom diameter, and bevel angle for these samples are (a) 800 nm, 472 nm, 68.5°; (b) 1.1 μm, 988 nm, 64.4°; (c) 1.5, 1.288 μm, 62.2°, respectively. The thicknesses of the metal and the dielectric are both fixed with $t_d = t_m = 40$ nm. Insets are 52°-tilted SEM images of the corresponding samples. The scale bar is 500 nm.

The period, bevel angle, and bottom diameter are denoted as P, θ, and w, respectively, as shown in the inset of Figure 1d.

RESULTS AND DISCUSSION

The proposed TCMA is independent of the incident polarization because of its inherent symmetry. For simplicity, only y-axis polarization incidence is applied in this paper, as illustrated in Figure 2a. Numerical simulations were performed using the frequency domain solver of the commercial software CST MICROWAVE STUDIO. The permittivity of gold (ε_m) is chosen by the Drude model with plasma frequency $\omega_p = 1.37 \times 10^{16}$ rad s^{-1} and damping rate $\gamma = 4.08 \times 10^{13}$ rad s^{-1}.[41] The permittivity of ZnO (ε_d) is extracted from ellipsometric measurements of ZnO films on silicon substrate. Periodic boundary conditions on both x- and y-directions are applied to characterize the periodic structures, and an open boundary is imposed in the z-direction. A gold film with a thickness of 100 nm is placed beneath the proposed nanostructure to block the transmission light, so the wavelength-dependent absorption $A(\lambda)$ could be calculated by $A(\lambda) = 1 - T(\lambda) - R(\lambda)$, where the transmittance $T(\lambda) = 0$. Figure 2b shows the simulated absorption spectrum for the TCMA with 10-pair plates using Au ($t_m = 20$ nm) and ZnO ($t_d = 40$ nm) under normal incidence. The period (P), bevel angle (θ), and bottom diameter (w) are 1 μm, 68.2°, and 800 nm, respectively. The simulated absorption spectrum indicates that the capability of light harvesting for TCMA absorbers is excellent with absorption higher than 90% covering the range from 1.7 to 3 μm. It is worth mentioning that the perfect absorption higher than 99% could be sustained over a broadband about 780 nm. Furthermore, the angular absorption spectra (see Figure 2c) clearly show that high and broadband absorption can be obtained even when the incident angle extends to 60°. It indicates that the absorption performance of the TCMA can be sustained in a wide incident angle range.

In order to confirm the design principle, we fabricate TCMA absorbers targeting the near-IR to mid-IR spectral regions. The absorption spectra are measured by a Fourier transform infrared spectrometer (Bruker HYPERION/VERTEX 80v), whose operating wavelength band is from 1.2 to 10 μm. The experimental reflection spectra are normalized with respect to a gold mirror. Here, the operating bandwidth of TCMA absorbers is defined as the spectral range where the absorption is higher than 70%. Figure 3 shows measured (blue) and simulated (red) absorption spectra for 5-pair Au−ZnO TCMA absorbers with different geometric parameters to trap light at multiband. When the period, bottom diameter, and bevel angle are 800, 472 nm, and 68.5°, respectively, the TCMA absorber operates at near-IR range, as shown in Figure 3a. The observed wavelength shift between experimental and simulation results is mainly attributed to the Drude model diverging from deposited materials in near-IR, where Au film suffers from high nonradiative losses. The measured operating bandwidth is from 1.32 to 2.13 μm with the absorption peak exceeding 94%. By adjusting the period, bottom diameter, and bevel angle to 1.1 μm, 988 nm, 64.4°, respectively, the absorption band can be extended to longer wavelength. It can be observed in Figure 3b that the experimental operating bandwidth is a band range of 2.5−4.35 μm, which agrees well with the simulation results. To further shift the absorption band to MIR range, the TCMA absorber with larger geometrical sizes (the period, bottom diameter, and bevel angle are 1.5, 1.288 μm, and 62.2°,

DOI: 10.1021/acs.jpcc.9b01634
J. Phys. Chem. C 2019, 123, 13856−13862

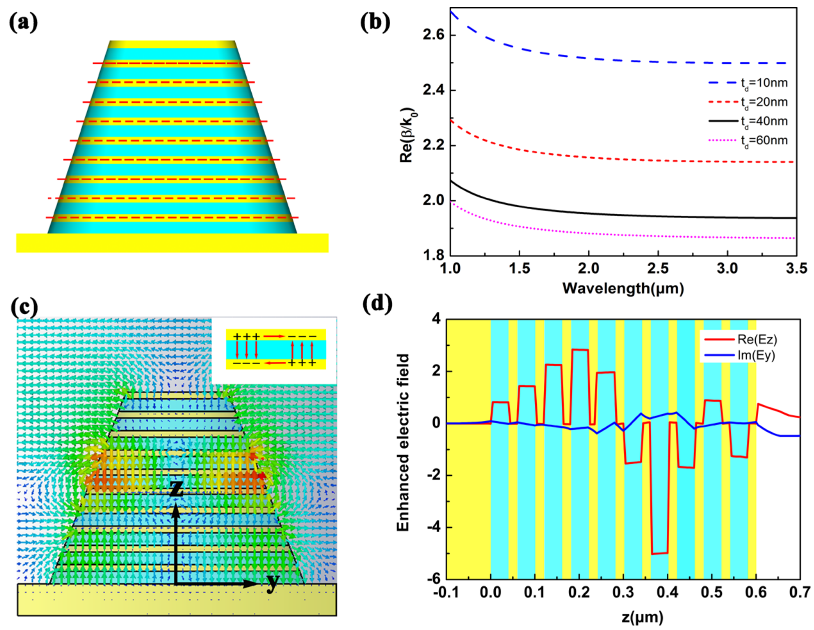

Figure 4. The multilayer metamaterial can be considered as a set of G-SPP resonators. (a) Schematic for TCMA decomposed into a set of MIM resonators; (b) Real part of the mode-index for G-SPP modes propagating primarily in a gap of thickness, t_d, between two gold films; (c) Electric field distributions in the plane of $x = 0$ at the wavelength of 2.4 μm, and the inset is the diagram of G-SPP mode in the individual MIM structure; (d) Distributions of electric field components at $y = 120$ nm in the plane of $x = 0$ for GPP modes supported by TCMA at the wavelength of 2.4 μm (t_m = 20 nm and t_d = 40 nm).

respectively) is fabricated. As shown in Figure 3c, the operating bandwidth can be tuned to 3.61−4.87 μm and the slight deviation is observed due to the fabrication imperfections and roughness of the prepared nanostructure. Through tailoring these geometrical parameters (P, w, and θ), the absorption bands of the TCMAs could be effectively extended to shorter or longer wavelength band.

To understand how broadband incident light is trapped by the TCMA, we will analyze the resonance modes and electric field distributions in the TCMA nanostructures with 10-pair Au−ZnO (t_m = 20 nm and t_d = 40 nm). There exist several metal−dielectric interfaces in the designed multilayer structures, which can sustain bound SPPs in the individual interfaces. As the thickness of the dielectric layer is smaller than the decay length of SPPs into the dielectric layer, interactions between SPPs result in coupled SPP modes in the dielectric layer, called gap SPP (G-SPP).[35−37] Therefore, the TCMA absorber can be considered as the combination of several symmetric Au−ZnO−Au (MIM) configurations with different sizes, as displayed in Figure 4a. The G-SPP existing in MIM structures is a type of electromagnetic wave that propagates parallel to the metal−dielectric interface and is confined perpendicular to the interface:

$$E(y, z) = E(z)e^{-i\beta y} \tag{1}$$

where β is the propagation constant of G-SPP modes. The G-SPP propagating in the MIM structure can be treated as a wave propagating in a uniform medium with a mode-index, $n_{eff} = \mathrm{Re}(\beta/k_0)$, which is the real part of the effective refractive index for G-SPP modes. The mode-index, as a function of the dielectric layer, t_d is shown in Figure 4b. The mode-index increases with the t_d decreasing, noting that the mode-index is higher than the refractive index of the dielectric material even when t_d = 60 nm. Figure 4c shows the electric field distributions of TCMA at the wavelength of 2.4 μm, and the inset is the electric field diagram of the G-SPP mode in an individual MIM structure. It indicates that the electric field distributions of assumptive MIM resonators in TCMA are consistent with those of G-SPP mode, proving that the G-SPP modes indeed exist in all dielectric layers of TCMA. The distributions of electric field components at $y = 120$ nm in the plane of $x = 0$ displayed in Figure 4d indicate strong confinement in all dielectric layers. Therefore, the TCMA nanostructures can support G-SPP modes with large mode-index and strong confinement in all dielectric layers. Compared with the previous theoretical analysis of slow-light modes,[31] we explain the high absorption from surface plasmon polariton in the individual interface, which can help in fundamental understanding of the absorption mechanism.

However, it's notable that there exists the strongest electric field distribution in a certain dielectric layer for a certain incident wavelength. This phenomenon can be explained in detail as follows. When the G-SPP modes reach the structure termination along the y-axis, it will be efficiently reflected due to the large mode-index and strong confinement. Constructive interference between backward and forward propagating G-SPPs results in standing-wave resonances, leading to larger field enhancement. That is to say, the assumptive MIM structure can operate as a Fabry−Perot-like resonator. Therefore, its resonance wavelength (λ) satisfies the following equation[38−40]

$$D\frac{2\pi}{\lambda}n_{eff} = m\pi - \phi \tag{2}$$

where n_{eff} is dependent on the geometric parameters, D is the average diameter of the Fabry−Perot-like resonator, ϕ is the reflection phase shift at the resonator termination, and m refers to the order of the resonance. Here, we focus on the lowest-order resonance ($m = 1$). The standing-wave resonance of G-SPP modes results in strong antiparallel electric field in the z-

DOI: 10.1021/acs.jpcc.9b01634
J. Phys. Chem. C 2019, 123, 13856−13862

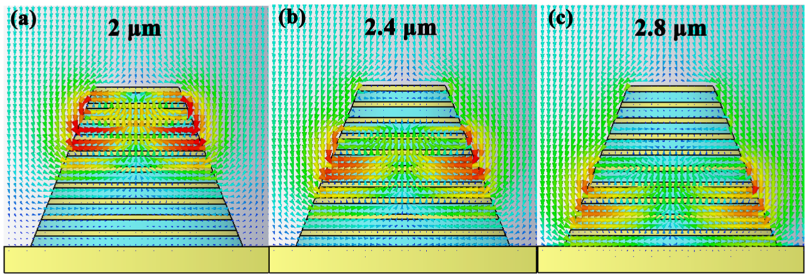

Figure 5. Light trapping in the multisized Fabry−Perot-like resonators of TCMA nanostructures. Distributions of the power flow in the plane of x = 0 at different wavelengths: (a) 2; (b) 2.4; and (c) 2.8 μm, respectively.

axis, which is much stronger than that in the y-axis, as shown in Figure 4c. The antiparallel electric field would form a circular field and generate magnetic dipole resonance. That is to say, the coupling of G-SPP modes in Fabry−Perot-like resonators leads to the enhancement of both electric and magnetic fields, which contributes to the high absorption. According to eq 2, it can be found that the resonance wavelength of the Fabry−Perot-like resonator has obviously monotonic correlation with the average diameter. That is to say, the incident light with a certain wavelength can be trapped by a Fabry−Perot-like resonator with certain diameter. The absorption mechanism based on Fabry−Perot-like resonators can well explain why the slow-light modes can exist in previous theoretical analysis and the wavelength of the resonance mode increases with the width of the resonator. The distributions of power flow in Figure 5 indicate that the position where the power is confined and light trapping occurs extends from top to bottom as the incident wavelength increases from 2 to 2.8 μm. Until the light trapping position extending to the bottom end, the cut-off of the absorption band emerges. For multilayered tapered TCMA nanostructures, the G-SPP modes excited by broad incident waves can be stood due to the multisized Fabry−Perot-like resonators, giving rise to efficient trapping of broadband incident light.

Based on the understanding of the optical absorption mechanism for TCMAs, the effect of period on the absorption performance is further discussed. As shown in Figure 6, the operating bandwidth and peak intensity of absorption spectra are both sensitive to the period. Higher absorptance and a broader absorption waveband are obtained by the smaller period. According to the above analysis of G-SPP modes supported in the TCMA structures, the G-SPP modes propagate along the y-axis and reflect at the structure termination. However, the energy of G-SPPs can be spatially concentrated in a region very close to the interface between the structure and air gap.[40] The y-component electric field (E_y) distributions in the inset of Figure 6 indicate that the field strength indeed concentrates in a region very close to the interface when the period is 2 μm. With the separation between adjacent unit cells decreasing, the leakage fields of GPPs between adjacent interfaces can couple with each other. It leads to the enhanced field distributions in the air gap and high absorption in the spectra, as shown in the E_y distributions and simulated absorption spectra for P = 0.9 μm. Therefore, it can be concluded that the enhanced localized field from the G-SPPs coupling in the air gap contributes to the high absorption in a broad waveband.

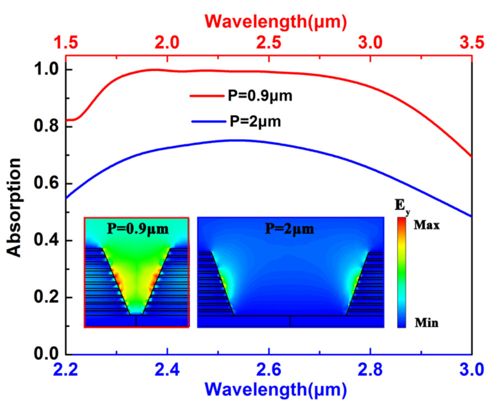

Figure 6. The simulated absorption spectra for TCMA nanostructures with different periods. The insets are the y-component electric field distributions in the plane of x = 0 for P = 0.9 μm and P = 2 μm at the incident wavelength of 2.5 μm, respectively. The geometric parameters are: N = 10, t_d = 20 nm, t_m = 40 nm, θ = 68.2°, and w = 1 μm.

■ CONCLUSIONS

In conclusion, we have demonstrated a Au−ZnO-stacked truncated-cone-type metamaterial, which exhibits broadband, polarization-insensitive, and wide-angle absorption. The TCMAs are fabricated by the combination of lithography and IBE techniques, which are both easily controllable and suitable for large-area fabrication. Because of the flexible adjustability of lithography and IBE techniques, the absorption band could be effectively tuned from near-IR to mid-IR range by tailoring the geometrical parameters (e.g., period, bevel angle, and bottom diameter). The tapered TCMA can be treated as a series of G-SPP resonators with varied diameters. Due to counter-propagating G-SPPs forming standing waves, stronger electric field is confined in the dielectric layers like Fabry−Perot resonators. These multisized Fabry−Perot-like resonators can trap multiwavelength incident light, giving rise to high and broadband absorption. By decreasing the separation of unit cells, the coupling between the leakage field of G-SPP modes in the adjacent nanostructures leads to strong electric field enhancement in the air gap, which contributes to broad and high absorption. This proposed metamaterial absorber offers various potential applications, such as solar cells and thermal emitters. What is more, the preparation method for TCMA provides a straightforward way to fabricate multilayer metamaterials with various structural morphologies.

■ AUTHOR INFORMATION

Corresponding Authors

*E-mail: jjli@iphy.ac.cn (J.L.).
*E-mail: czgu@iphy.ac.cn (C.G.).

DOI: 10.1021/acs.jpcc.9b01634
J. Phys. Chem. C 2019, 123, 13856−13862

ORCID

Sha Hu: 0000-0002-3851-8003

Shengyan Yang: 0000-0003-0667-3743

Junjie Li: 0000-0002-1508-9891

Changzhi Gu: 0000-0002-2689-2807

Author Contributions

S. Hu and S. Yang contributed equally to this work. The manuscript was written through contributions of all authors. All authors have given approval to the final version of the manuscript.

Notes

The authors declare no competing financial interest.

■ ACKNOWLEDGMENTS

This work was supported by the National Key Research and Development Program of China (grant nos. 2016YFA0200400, 2016YFA0200800), National Natural Science Foundation of China (grant nos. 11674387, 91323304, 11504414, 11574369, 11574385, 11574368, 61888102), Strategic Priority Research Program, and Key Research Program of Frontier Sciences of Chinese Academy of Sciences (grant nos. XDB07020200, QYZDJ-SSW-SLH042).

■ REFERENCES

(1) Cai, W.; Shalaev, V. *Optical Metamaterials*; Springer: New York, USA, 2010.

(2) Sihvola, A. Metamaterials in electromagnetics. *Metamaterials* **2007**, *1*, 2−11.

(3) Smith, D. R.; Pendry, J. B.; Wiltshire, M. C. Metamaterials and negative refractive index. *Science* **2004**, *305*, 788−792.

(4) Pendry, J. B. Negative refraction makes a perfect lens. *Phys. Rev. Lett.* **2000**, *85*, 3966−3969.

(5) Yang, S.; Xia, X.; Liu, Z.; Yiwen, E.; Wang, Y.; Tang, C.; Li, W.; Li, J.; Wang, L.; Gu, C. Multispectral plasmon-induced transparency in hyperfine terahertz meta-molecules. *J. Phys.: Condens. Matter* **2016**, *28*, 445002.

(6) Hu, S.; Yang, S.; Liu, Z.; Li, J.; Gu, C. Broadband cross-polarization conversion by symmetry-breaking ultrathin metasurfaces. *Appl. Phys. Lett.* **2017**, *111*, 241108.

(7) Landy, N. I.; Sajuyigbe, S.; Mock, J. J.; Smith, D. R.; Padilla, W. J. Perfect metamaterial absorber. *Phys. Rev. Lett.* **2008**, *100*, 207402.

(8) Wang, Y.; Sun, T.; Paudel, T.; Zhang, Y.; Ren, Z.; Kempa, K. Metamaterial-plasmonic absorber structure for high efficiency amorphous silicon solar cells. *Nano Lett.* **2012**, *12*, 440−445.

(9) Chen, J.-D.; Li, Y.-Q.; Zhu, J.; Zhang, Q.; Xu, R.-P.; Li, C.; Zhang, Y.-X.; Huang, J.-S.; Zhan, X.; You, W.; Tang, J.-X. Polymer solar cells with 90% external quantum efficiency featuring an ideal light- and charge-manipulation layer. *Adv. Mater.* **2018**, *30*, 1706083.

(10) Rephaeli, E.; Fan, S. Absorber and emitter for solar thermo-photovoltaic systems to achieve efficiency exceeding the Shockley-Queisser limit. *Opt. Express* **2009**, *17*, 15145−15159.

(11) Liu, N.; Mesch, M.; Weiss, T.; Hentschel, M.; Giessen, H. Infrared perfect absorber and its application as plasmonic sensor. *Nano Lett.* **2010**, *10*, 2342−2348.

(12) Hu, X.; Xu, G.; Wen, L.; Wang, H.; Zhao, Y.; Zhang, Y.; Cumming, D. R. S.; Chen, Q. Metamaterial absorber integrated microfluidic terahertz sensors. *Laser Photonics Rev.* **2016**, *10*, 962−969.

(13) Cong, L.; Tan, S.; Yahiaoui, R.; Yan, F.; Zhang, W.; Singh, R. Experimental demonstration of ultrasensitive sensing with terahertz metamaterial absorbers: A comparison with the metasurfaces. *Appl. Phys. Lett.* **2015**, *106*, 031107.

(14) Wu, P. C.; Liao, C. Y.; Chen, J.-W.; Tsai, D. P. Isotropic absorption and sensor of vertical split-ring resonator. *Adv. Opt. Mater.* **2017**, *5*, 1600581.

(15) Liu, X.; Starr, T.; Starr, A. F.; Padilla, W. J. Infrared spatial and frequency selective metamaterial with near-unity absorbance. *Phys. Rev. Lett.* **2010**, *104*, 207403.

(16) Landy, N. I.; Bingham, C. M.; Tyler, T.; Jokerst, N.; Smith, D. R.; Padilla, W. J. Design, theory, and measurement of a polarization-insensitive absorber for terahertz imaging. *Phys. Rev. B: Condens. Matter Mater. Phys.* **2009**, *79*, 125104.

(17) Wang, H.; Yang, Y.; Wang, L. Switchable wavelength-selective and diffuse metamaterial absorber/emitter with a phase transition spacer layer. *Appl. Phys. Lett.* **2014**, *105*, 071907.

(18) Xu, H.-X.; Wang, G.-M.; Qi, M.-Q.; Liang, J.-G.; Gong, J.-Q.; Xu, Z.-M. Triple-band polarization-insensitive wide-angle ultra-miniature metamaterial transmission line absorber. *Phys. Rev. B: Condens. Matter Mater. Phys.* **2012**, *86*, 205104.

(19) Liu, X.; Tyler, T.; Starr, T.; Starr, A. F.; Jokerst, N. M.; Padilla, W. J. Taming the blackbody with infrared metamaterials as selective thermal emitters. *Phys. Rev. Lett.* **2011**, *107*, 045901.

(20) Feng, R.; Qiu, J.; Liu, L.; Ding, W.; Chen, L. Parallel LC circuit model for multi-band absorption and preliminary design of radiative cooling. *Opt. Express* **2014**, *22*, A1713−A1724.

(21) Shen, X.; Yang, Y.; Zang, Y.; Gu, J.; Han, J.; Zhang, W.; Cui, T. J. Triple-band terahertz metamaterial absorber: Design, experiment, and physical interpretation. *Appl. Phys. Lett.* **2012**, *101*, 154102.

(22) Wen, Q.-Y.; Zhang, H.-W.; Xie, Y.-S.; Yang, Q.-H.; Liu, Y.-L. Dual band terahertz metamaterial absorber: Design, fabrication, and characterization. *Appl. Phys. Lett.* **2009**, *95*, 241111.

(23) Bossard, J. A.; Lin, L.; Yun, S.; Liu, L.; Werner, D. H.; Mayer, T. S. Near-ideal optical metamaterial absorbers with super-octave bandwidth. *ACS Nano* **2014**, *8*, 1517−1524.

(24) Kenney, M.; Grant, J.; Shah, Y. D.; Escorcia-Carranza, I.; Humphreys, M.; Cumming, D. R. S. Octave-spanning broadband absorption of terahertz light using metasurface fractal-cross absorbers. *ACS Photonics* **2017**, *4*, 2604−2612.

(25) Guo, W.; Liu, Y.; Han, T. Ultra-broadband infrared metasurface absorber. *Opt. Express* **2016**, *24*, 20586−20592.

(26) Butun, S.; Aydin, K. Structurally tunable resonant absorption bands in ultrathin broadband plasmonic absorbers. *Opt. Express* **2014**, *22*, 19457−19468.

(27) Zhang, C.; Cheng, Q.; Yang, J.; Zhao, J.; Cui, T. J. Broadband metamaterial for optical transparency and microwave absorption. *Appl. Phys. Lett.* **2017**, *110*, 143511.

(28) Ding, F.; Cui, Y.; Ge, X.; Jin, Y.; He, S. Ultra-broadband microwave metamaterial absorber. *Appl. Phys. Lett.* **2012**, *100*, 103506.

(29) Kim, Y. J.; Yoo, Y. J.; Kim, W. K.; Rhee, J. Y.; Kim, Y. H.; Lee, Y. Dual broadband metamaterial absorber. *Opt. Express* **2015**, *23*, 3861−3868.

(30) Yang, J.; Hu, X.; Li, X.; Liu, Z.; Liang, Z.; Jiang, X.; Zi, J. Broadband absorption enhancement in anisotropic metamaterials by mirror reflections. *Phys. Rev. B: Condens. Matter Mater. Phys.* **2009**, *80*, 125103.

(31) Cui, Y.; Fung, K. H.; Xu, J.; Ma, H.; Jin, Y.; He, S.; Fang, N. X. Ultrabroadband light absorption by a sawtooth anisotropic metamaterial slab. *Nano Lett.* **2012**, *12*, 1443−1447.

(32) Liang, Q.; Wang, T.; Lu, Z.; Sun, Q.; Fu, Y.; Yu, W. Metamaterial-based two dimensional plasmonic subwavelength structures offer the broadest waveband light harvesting. *Adv. Opt. Mater.* **2013**, *1*, 43−49.

(33) Ji, D.; Song, H.; Zeng, X.; Hu, H.; Liu, K.; Zhang, N.; Gan, Q. Broadband absorption engineering of hyperbolic metafilm patterns. *Sci. Rep.* **2014**, *4*, 4498.

(34) Zhou, J.; Kaplan, A. F.; Chen, L.; Guo, L. J. Experiment and theory of the broadband absorption by a tapered hyperbolic metamaterial array. *ACS Photonics* **2014**, *1*, 618−624.

(35) Bozhevolnyi, S. I.; Sondergaard, T. General properties of slow-plasmon resonant nanostructures: nano-antennas and resonators. *Opt. Express* **2007**, *15*, 10869−10877.

DOI: 10.1021/acs.jpcc.9b01634
J. Phys. Chem. C 2019, 123, 13856−13862

(36) Pakizeh, T.; Abrishamian, M. S.; Granpayeh, N.; Dmitriev, A.; Käll, M. Magnetic-field enhancement in gold nanosandwiches. *Opt. Express* **2006**, *14*, 8240−8246.
(37) Jung, J.; Søndergaard, T. Gap plasmon-polariton nanoresonators: Scattering enhancement and launching of surface plasmon polaritons. *Phys. Rev. B: Condens. Matter Mater. Phys.* **2009**, *79*, 035401.
(38) Søndergaard, T.; Jung, J.; Bozhevolnyi, S. I.; Valle, G. D. Theoretical analysis of gold nano-strip gap plasmon resonators. *New J. Phys.* **2008**, *10*, 105008.
(39) Gordon, R. Light in a subwavelength slit in a metal: Propagation and reflection. *Phys. Rev. B: Condens. Matter Mater. Phys.* **2006**, *73*, 153405.
(40) Pros, A.; Bozhevolnyi, S. I. Plasmonic metasurfaces for efficient phase control in reflection. *Opt. Express* **2013**, *21*, 27438−27451.
(41) Yang, S.; Tang, C.; Liu, Z.; Wang, B.; Wang, C.; Li, J.; Wang, L.; Gu, C. Simultaneous excitation of extremely high-Q-factor trapped and octupolar modes in terahertz metamaterials. *Opt. Express* **2017**, *25*, 15938−15946.

DOI: 10.1021/acs.jpcc.9b01634
J. Phys. Chem. C 2019, 123, 13856−13862